Supporting Information

Acetylacetone as an axial ligand in metalloporphyrin: the first crystal structure, coordination chemistry, and potential application as efficient photosensitizer

Abdul K. Choudhury [a] and Jagannath Bhuyan *[a,b]

[a] Department of Chemistry, North Eastern Regional Institute of Science and Technology, Nirjuli, Arunachal Pradesh- 791109, India

[b] Department of Chemistry, Bhattadev University, Bajali, Pathsala, Assam-781325, India

E-mail: jnb@nersit.ac.in

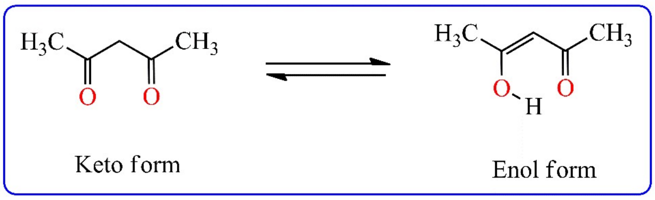

Figure S1. Structure of acetylacetone (keto-enol tautomerism).

Synthesis of ligand 5,10,15,20-tetrakis-(4-chlorophenyl)porphyrin, $H_2T(4\text{-}Cl)PP$

The ligand 5,10,15,20-tetrakis-(4-chlorophenyl)porphyrin, $H_2T(4\text{-}Cl)PP$ (Scheme 4.2) was prepared by refluxing 10.13 g 4-chlorobenzaldehyde (72 mmol) and 5 mL pyrrole (72 mmol) in 250 mL propionic acid following the reported procedure[38]. The yield of the compound was 20%. Molecular Formula: $C_{44}H_{26}Cl_4N_4$; Molecular Weight: 752.52; Elemental analysis calcd. (%) for $C_{44}H_{26}Cl_4N_4$: C 70.23, H 3.48, N 7.45; Found: C 70.32, H 3.53, N 7.50; UV/Visible bands are at λ_{max}/nm (ε/ $Lmol^{-1}cm^{-1}$) (in CH_2Cl_2, 10^{-6} M): 418 (584000 $Lmol^{-1}cm^{-1}$), 514 (40000 $Lmol^{-1}cm^{-1}$), 549 (24000 $Lmol^{-1}cm^{-1}$), 589 (19200 $Lmol^{-1}$ cm^{-1}) and 647 (16800 $Lmol^{-1}cm^{-1}$), respectively, FTIR (KBr disc) cm^{-1}: 3322($\nu_{N–H,\ pyrrole}$), 3020($\nu_{C–H,\ aromatic}$), 2333($\nu_{C=C}$), 1679($\nu_{C=C,\ pyrrole}$), 1165($\nu_{C–H,\ pyrrole}$), 1468 [$\nu_{C\text{-}C\ (Bz)}$], 1394[$\nu_{Cp\text{-}N}$], 852 [$\delta_{Cp\text{-}Cp,}$], 799($\nu_{C–Cl}$), 735 [Л$_{C\text{-}H}$].

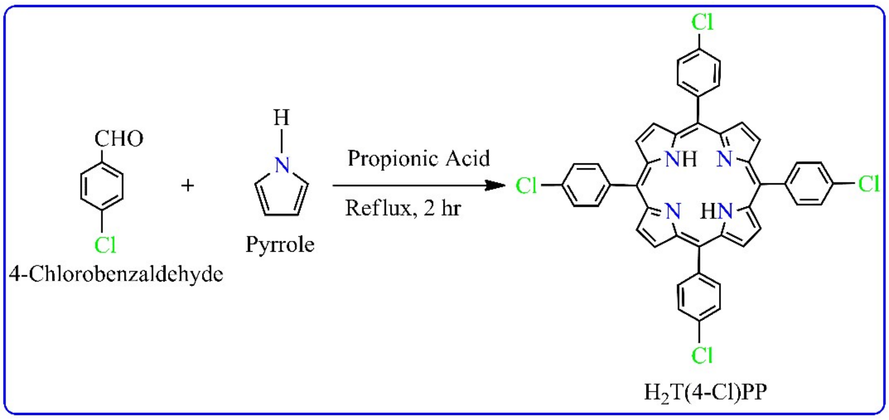

Scheme S1. Synthesis of ligand.

Synthesis of 5,10,15,20-tetrakis-(4-chlorophenyl)porphyrinato magnesium(II), $Mg^{II}T(4\text{-}Cl)PP$

A sample of 1 g (1.33 mmol) $H_2T(4\text{-}Cl)PP$ and 0.713 g (3.32 mmol) $Mg(CH_3COO)_2.4H_2O$ was refluxed for 1 hour in 50 mL DMF in a round bottom flask. Then 30 mg sodium acetate was added, and the mixture was refluxed for another 6 hours (the completion of metalation was monitored by UV-Vis spectroscopy). Then the solvent was evaporated, and the solid residue was dissolved in DCM, filtered, and dried. The compound was isolated and purified by column chromatography over neutral alumina using eluent DCM-acetone (9:1). Yield: 80%. Molecular Formula: $C_{44}H_{24}Cl_4$ MgN_4; Molecular Weight: 774.81; UV/Vis (in CH_2Cl_2) λmax/nm (ε): 425 (608000 $Lmol^{-1}cm^{-1}$), 563 (32000 $Lmol^{-1}cm^{-1}$), 603 (20800 $Lmol^{-1}cm^{-1}$); Elemental analysis calcd. (%) for $C_{44}H_{24}Cl_4$ MgN_4: C 68.21, H 3.12, N 7.23; Found: C 68.30, H 3.17, N 7.28; FTIR (KBr disk) cm^{-1}: 2962($\nu_{C–H,\ aromatic}$), 1665($\nu_{C=C}$), 1478($\nu_{C=C}$,pyrrole), 1379($\nu_{C–N}$), 1175($\nu_{C–Hpyrrole}$), 793($\nu_{C\text{-}Cl}$), 470($\nu_{Mg\text{-}N\ por}$).

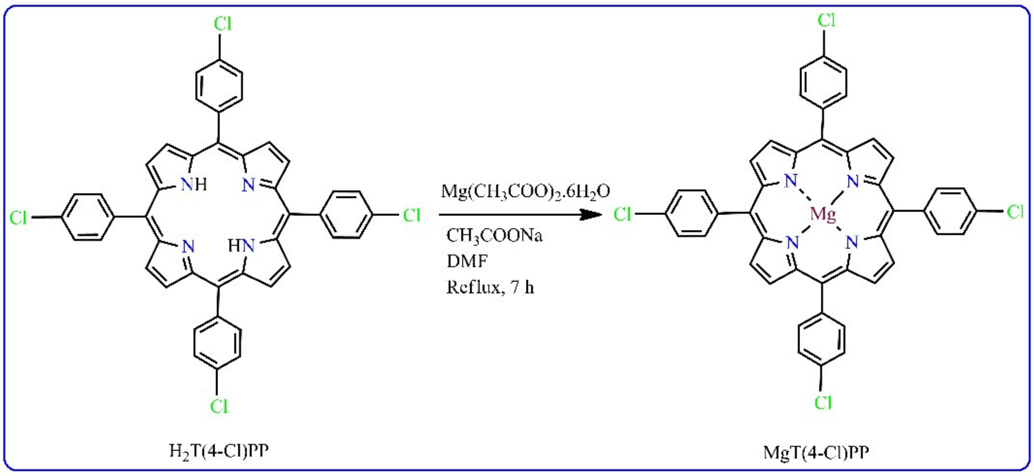

Scheme S2. Synthesis of MgT(4-Cl)PP.

Table S1. Selected experimental and theoretical (optimized) (i) bond lengths (Å) and (ii)angles (°) of compound **1**

(i) Bond lengths(Å)	**Crystal structure**	**Optimized structure**
Mg1–N1	2.083(3)	2.096
Mg1–N2	2.092(4)	2.092
Mg1–N3	2.079(3)	2.092
Mg1–N4	2.087(4)	2.093
Mg1–O1	2.073(4)	2.118
O1–C45	1.254(6)	1.294
O2–C48	1.317(6)	1.349
(ii)Angles (°)	**Crystal structure**	**Optimized structure**
O1–Mg1–N1	103.52(14)	101.76
O1–Mg1–N2	104.78(15)	103.19
O1–Mg1–N3	99.71(14)	95.66
O1–Mg1–N4	96.48(15)	93.04
N1–Mg1–N2	87.93(14)	88.69
N1–Mg1–N3	156.73(15)	162.53
N1–Mg1–N4	87.49(14)	88.74
N2–Mg1–N3	87.69(14)	88.98
N2–Mg1–N4	158.73(16)	163.74

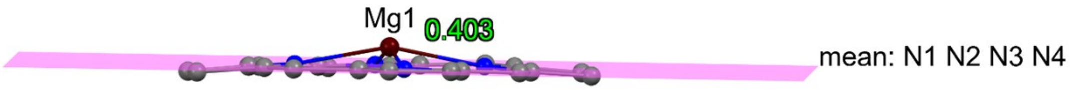

Figure S2. Displacement of the Mg atom from the mean porphyrin plane.

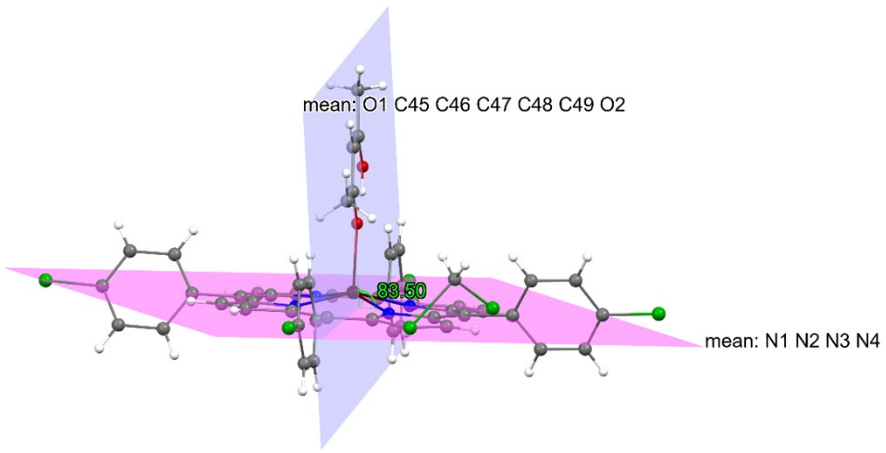

Figure S3. Angle between porphyrin mean plane and axial pyrazine plane.

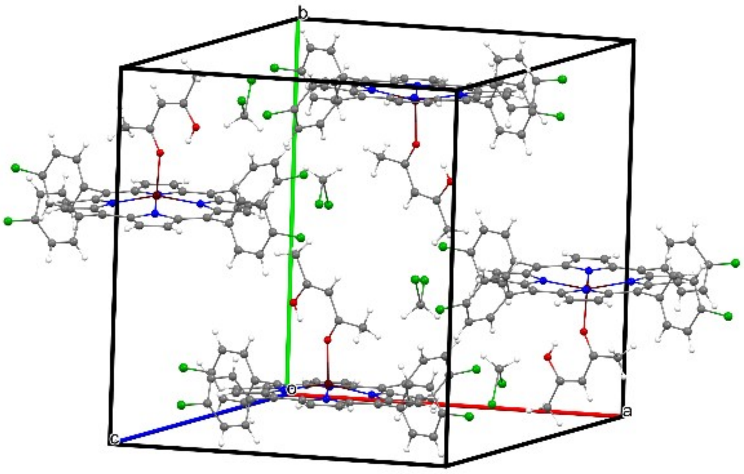

Figure S4. Crystal packing diagram of compound **1** along b-axis.

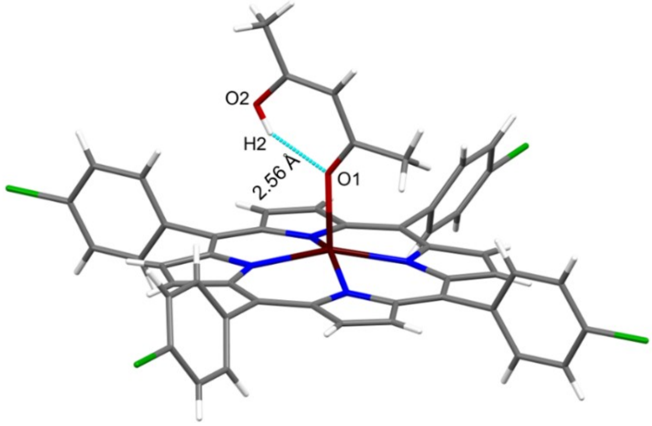

Figure S5. Intra-molecular H-bonding in compound **1.**

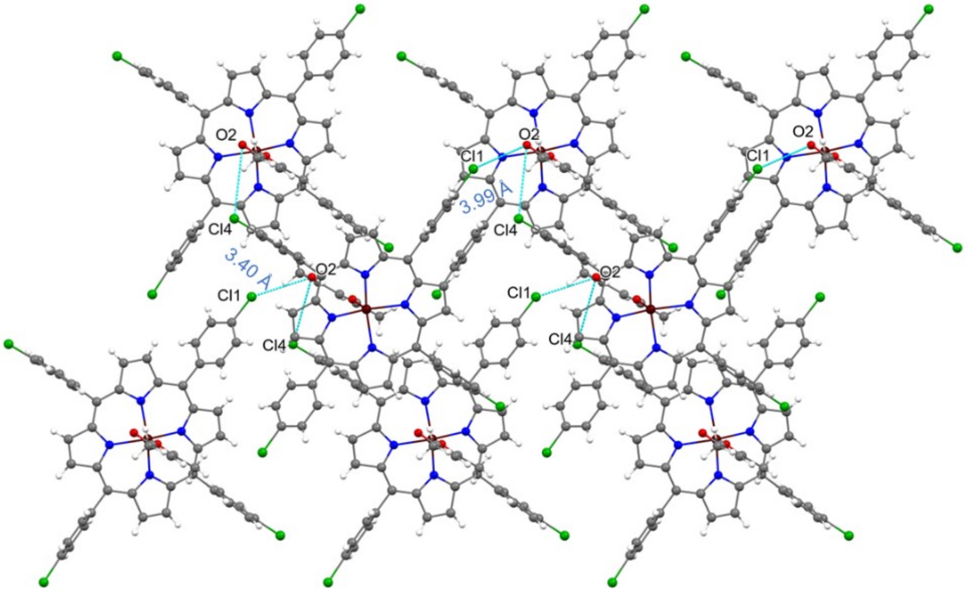

Figure S6. Supramolecular self-assembly in **1** due to Cl···O_{Hacac} halogen-bonding interactions.

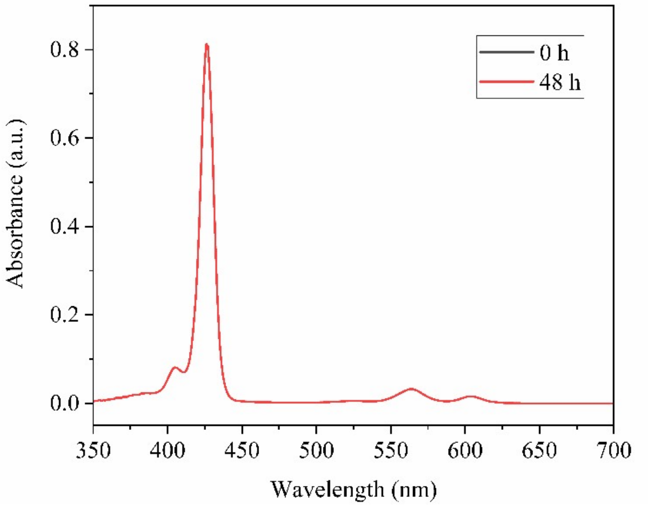

Figure S7. UV-Vis spectra for the stability study of compound **1** in DCM solution over 48 hours.

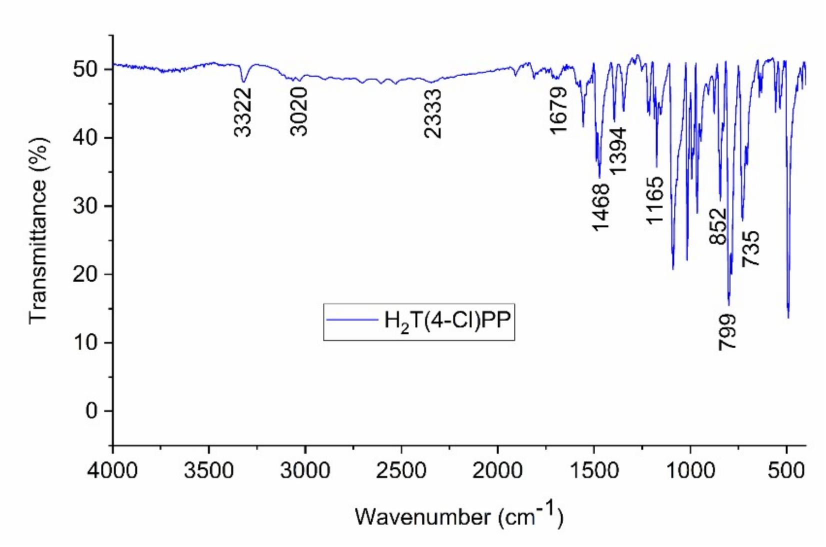

Figure S8. IR spectrum of $H_2T(4\text{-}Cl)PP$.

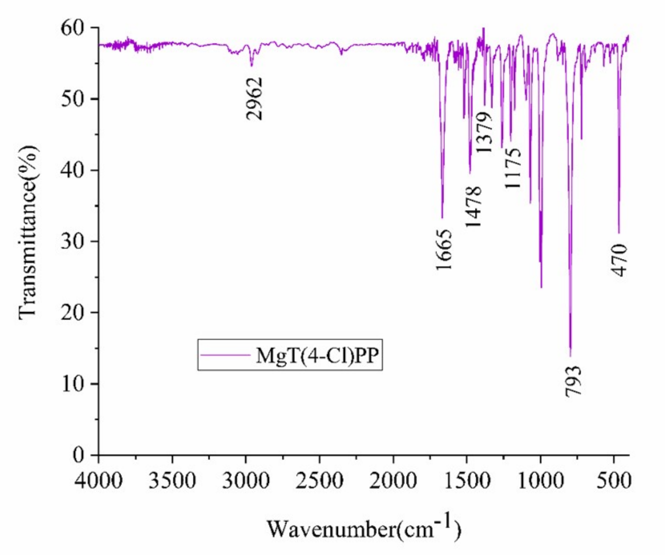

Figure S9. IR spectrum of MgT(4-Cl)PP.

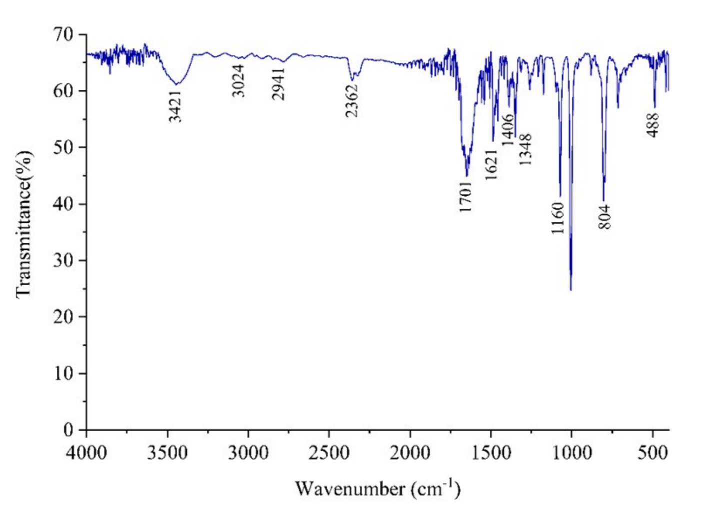

Figure S0. IR spectrum of **1**.

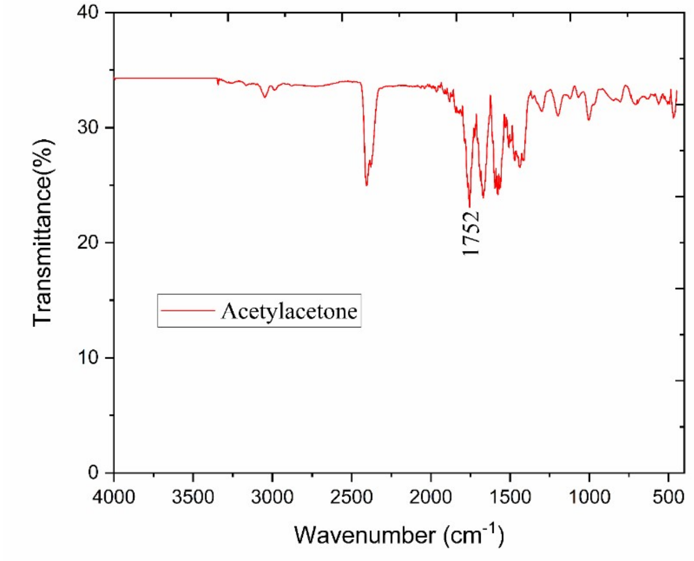

Figure S11. IR spectrum of free acetylacetone.

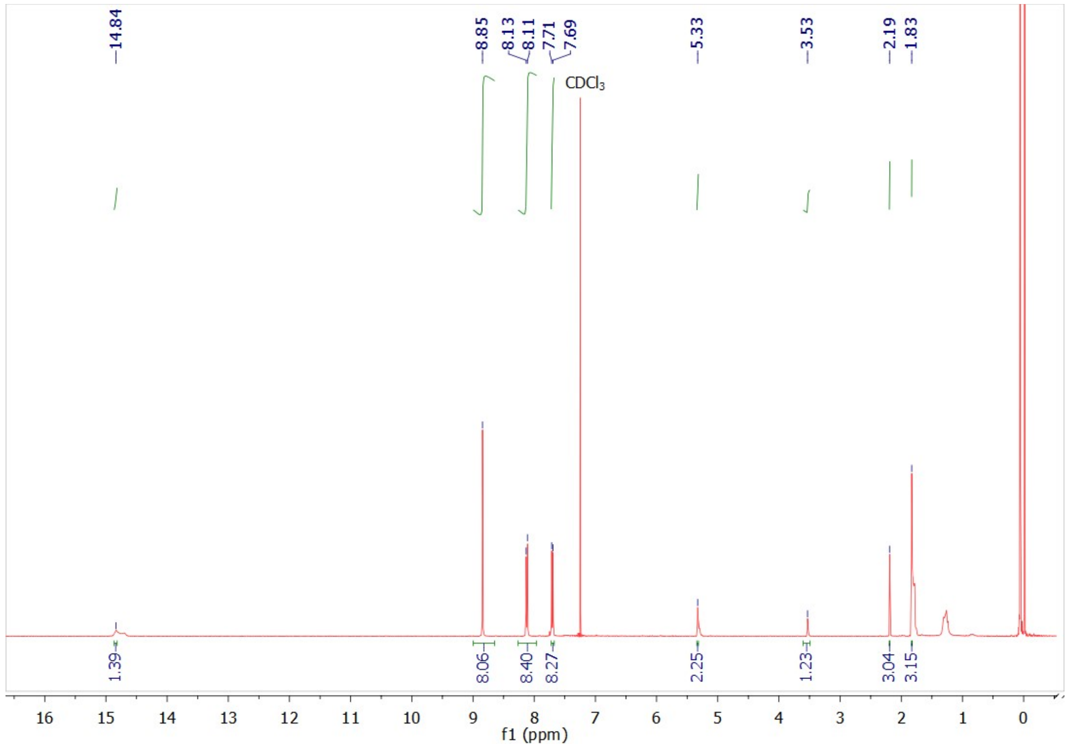

Figure S12. ^{1}HNMR spectrum of **1**.

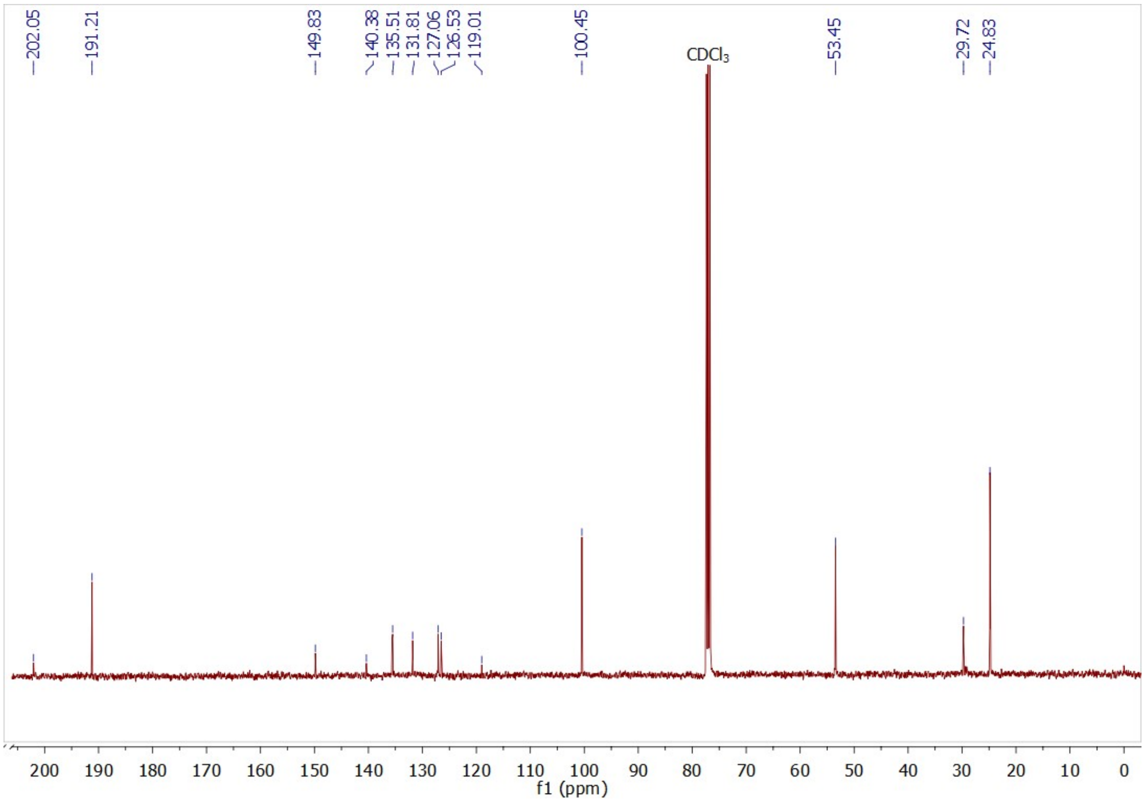

Figure S13. ^{13}C NMR spectrum of **1**.

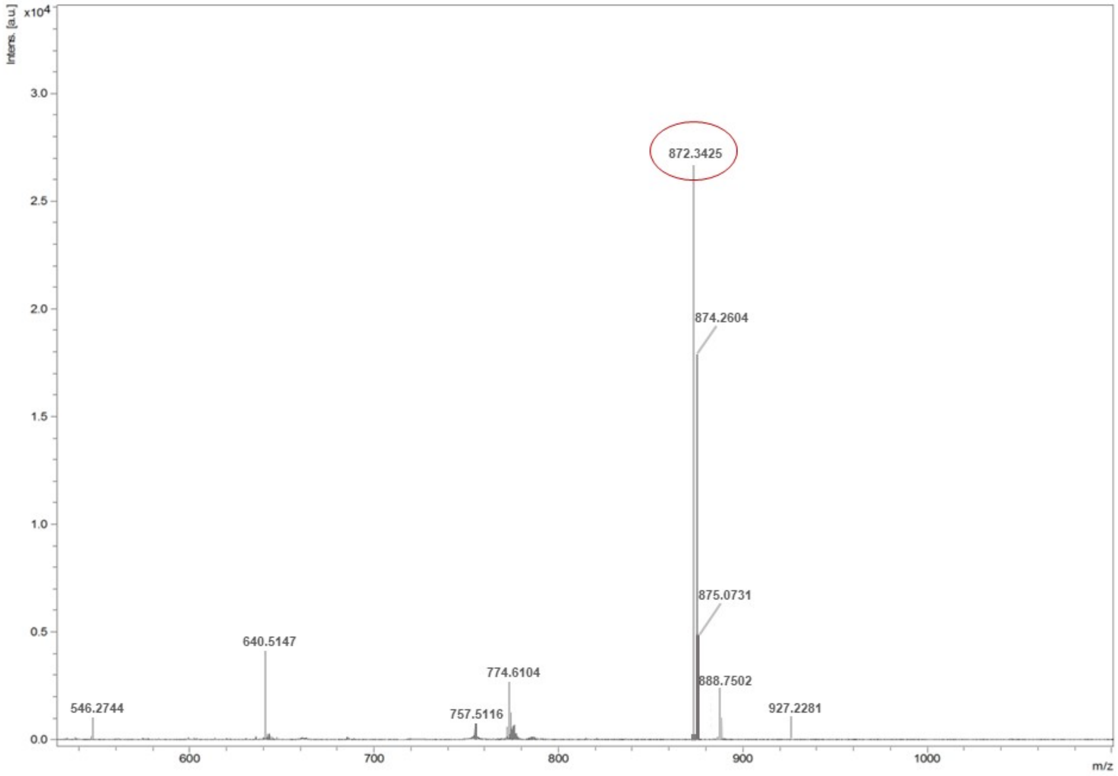

Figure S14. MALDI-TOF MS spectrum of **1**.

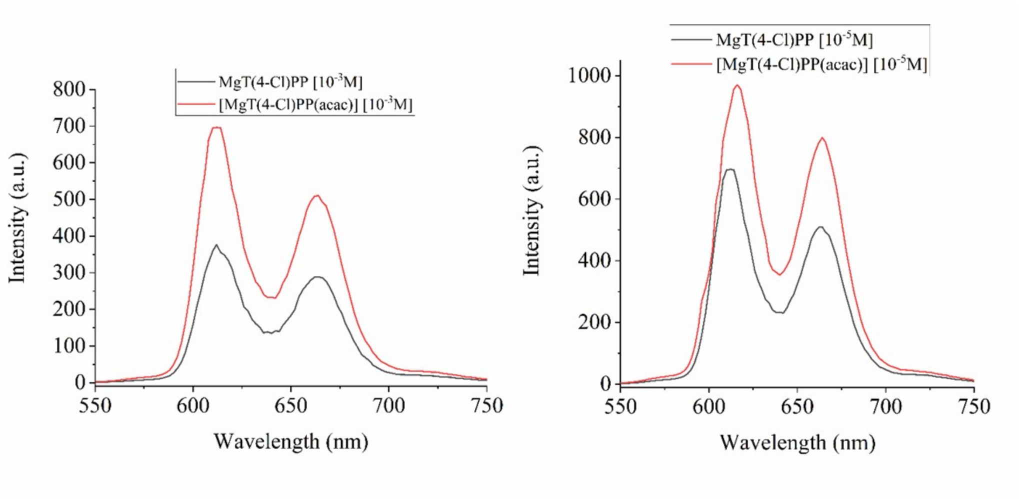

Figure S15. Emission spectra of MgT(4-Cl)PP and **1** at two different concentrations in DCM (λ_{ex} = 420 nm) at room temperature.

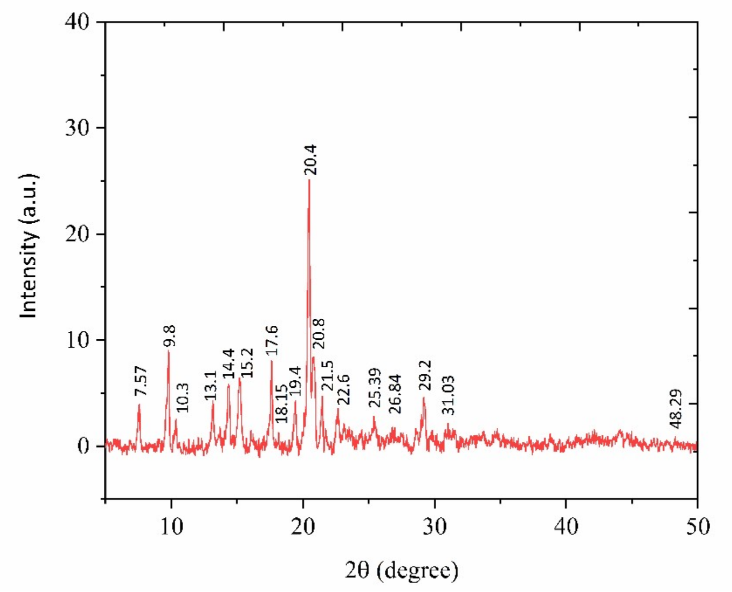

Figure S16. Powder X-ray diffraction spectrum of compound 1.

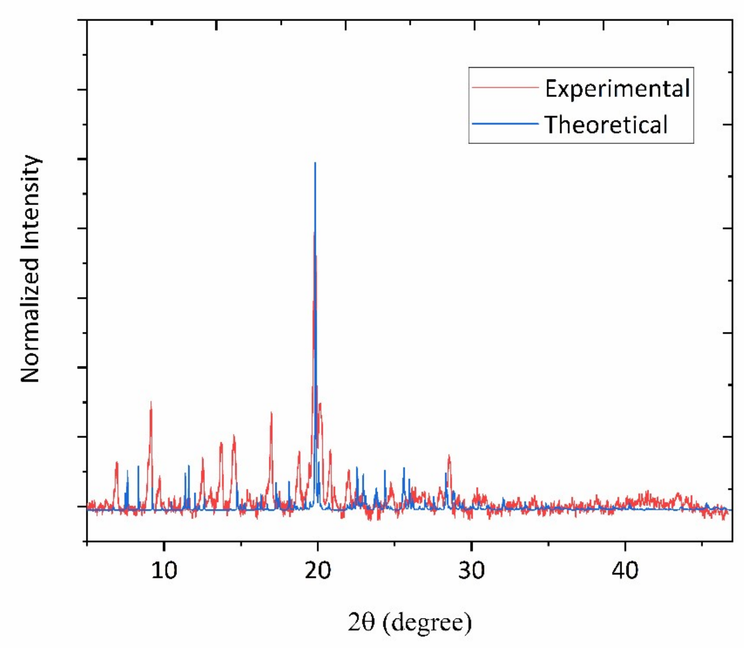

Figure S17. Comparison of experimental and theoretical Powder XRD spectra of compound 1.

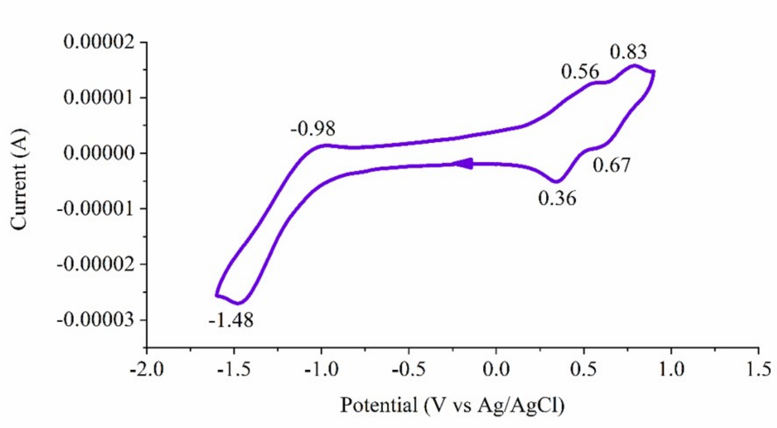

Figure S18. Cyclic voltammogram of MgT(4-Cl)PP (10^{-3} M) in dry DCM with scan rate 0.1 V/s.

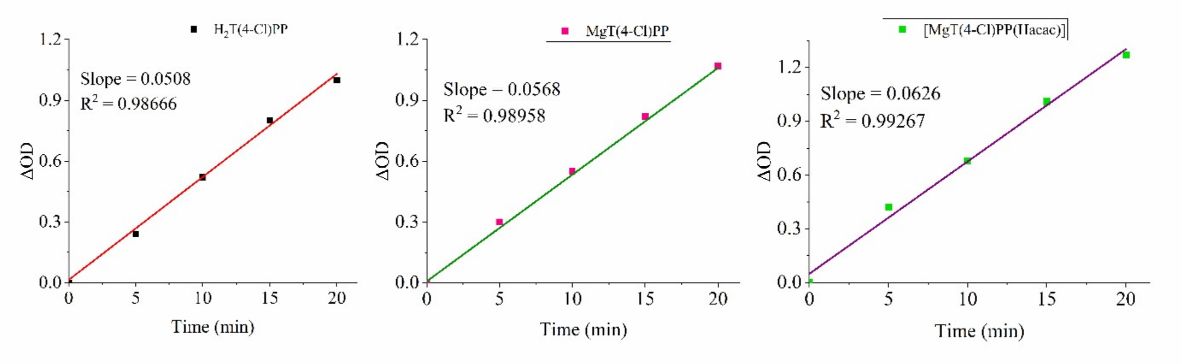

Figure S19. Plot of optical density of DPBF with time.

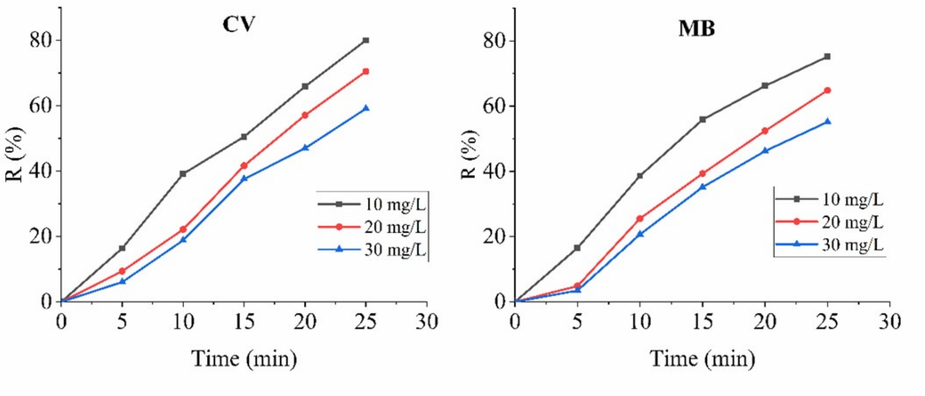

Figure S20. Adsorption efficiency curves of CV and MB dye as a function of time of the compound **1** (m = 10 mg/L, pH = 7).

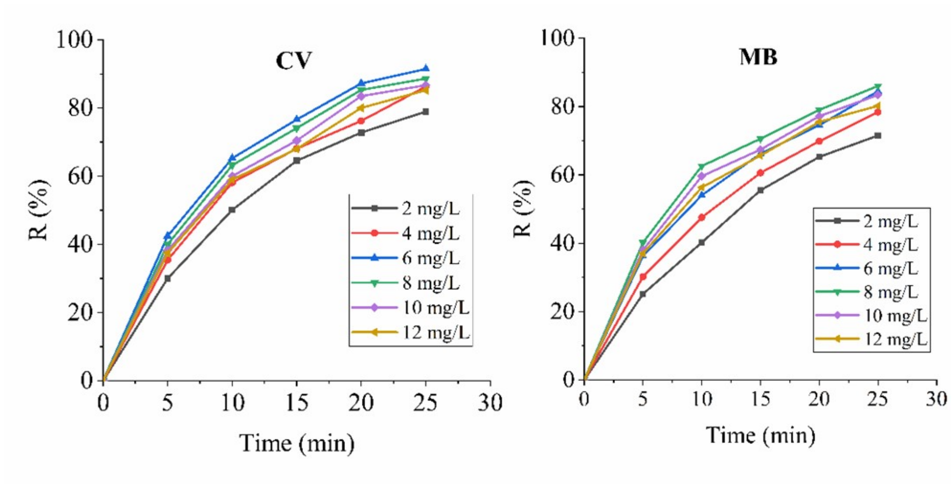

Figure S21. Change in the degradation efficiency of the CV (10mg/L) and MB (10mg/L) dye as a function of time of the compound **1** (m = 2-12 mg/L, pH=7).

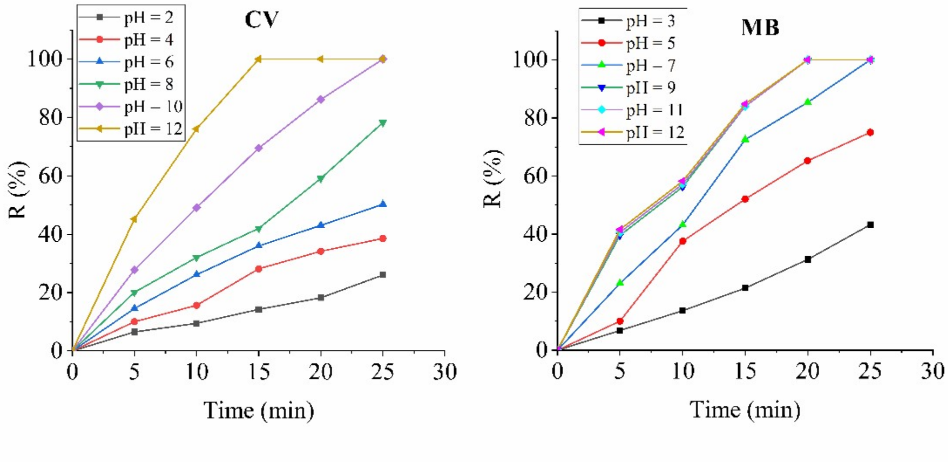

Figure S22. Change in the degradation efficiency of the CV (10mg/L) and MB (10mg/L) dye as a function of time of the compound **1** (m = 6 mg/L for CV and 8mg/L for MB) on varying pH (2-12).

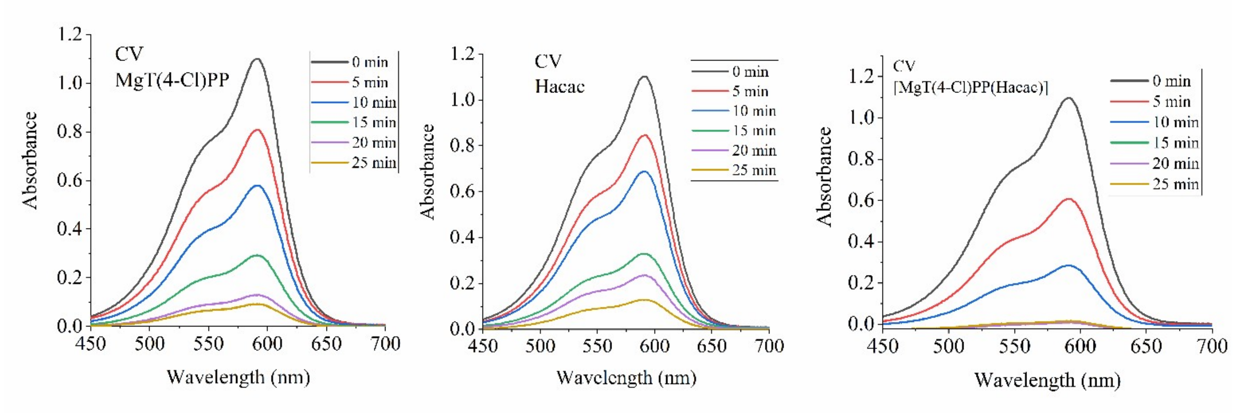

Figure S23. Change in absorption intensity at different intervals of time on irradiation of aqueous solution of CV dye in presence of catalysts MgT(4-Cl)PP, Hacac and **1.**

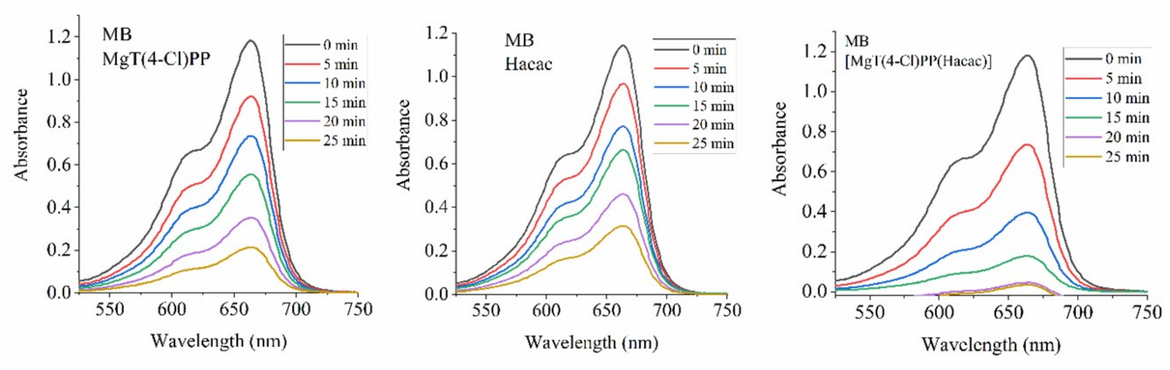

Figure S24. Change in absorption intensity at different intervals of time on irradiation of aqueous solution of MB dye in presence of catalysts MgT(4-Cl)PP, Hacac and **1**.

Table S2. Comparison of photocatalytic degradation efficiency of some reported compounds in different dyes.

Compound	**Pollutant**	**Light source**	**Irradiation time**	**Degradation yield**	**Reference**
ZnTMPyP−GO	Rhodamine B	Visible-light	120 min	19%	48
Zirconium MOF nanosheets using Ni porphyrin	Nitrotoluene	Visible-light	60 min	100%	49
	Nitrobenzene		90 min	100%	
	Chloronitrobenzene		105 min	100 %	
0.5 mol% Cd doped ZnO	Crystal violet (CV)	UV	30 min	100 %	50

		Chamber (06 W)			
(4%) Cd-ZnO	Methylene blue (MB)	Sunlight	30 min	84 %	51
[Co^{II}(TBrPP)(DMAP)$_2$]	Toluidine blue	Visible light	90 min	84.8 %	52
[Co^{II}(TClPP)(DMAP)$_2$]				86.9 %	
MgT(4-Cl)PP	CV	Sunlight	15 min	74.88%	This work
	MB		20 min	70.54%	
[MgT(4-Cl)PP(Hacac)], **1**	CV	Sunlight	15 min	100 %	This work
	MB		20 min		

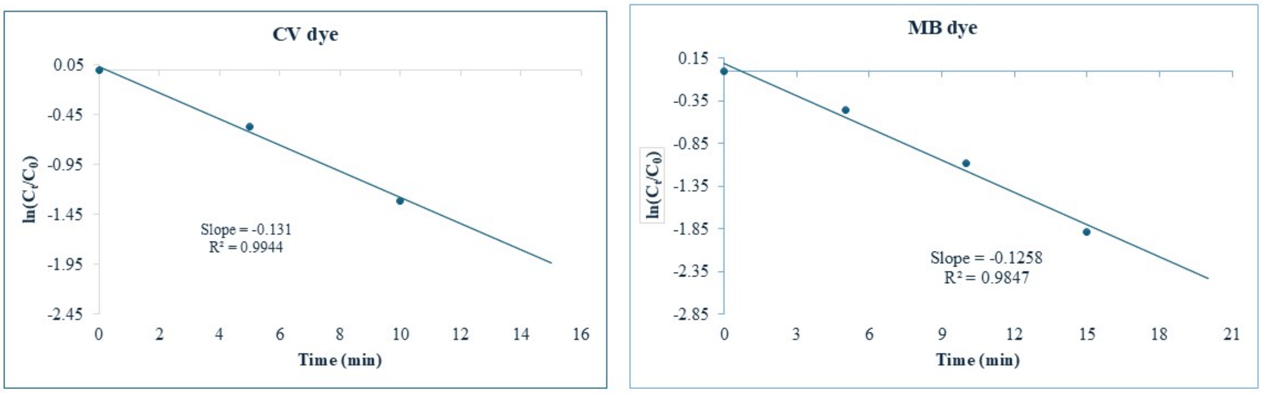

(a) (b)

Figure S25. Plot of ln(C_t /C_o) vs time showing the pseudo-first-order reaction kinetics of CV (a) and MB (b) dye degradation.

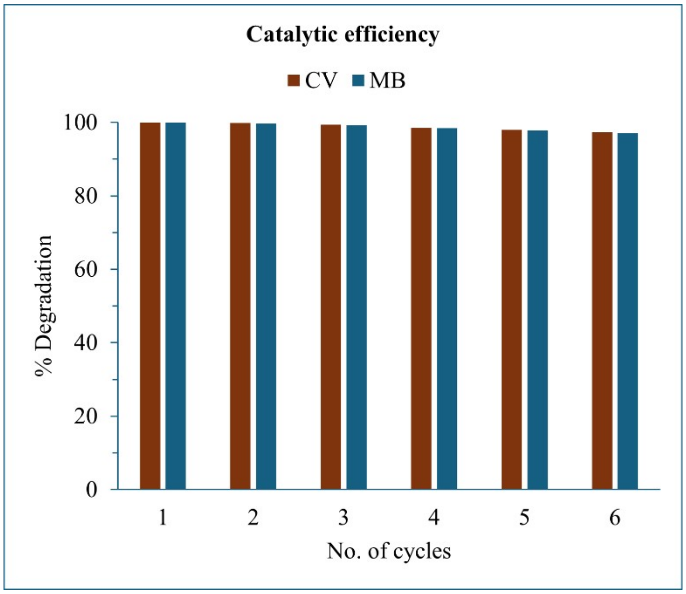

Figure S26. Photocatalytic stability of **1** in CV and MB dye.

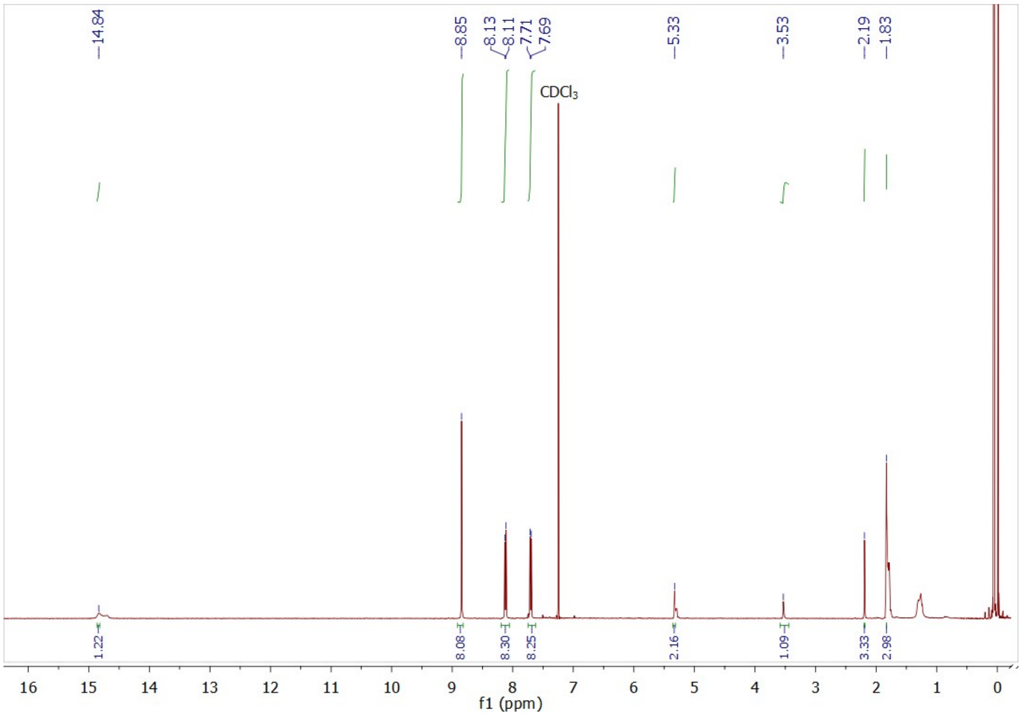

Figure S27. ^{1}H NMR spectrum of catalyst **1** after degradation of CV dye over six cycles.

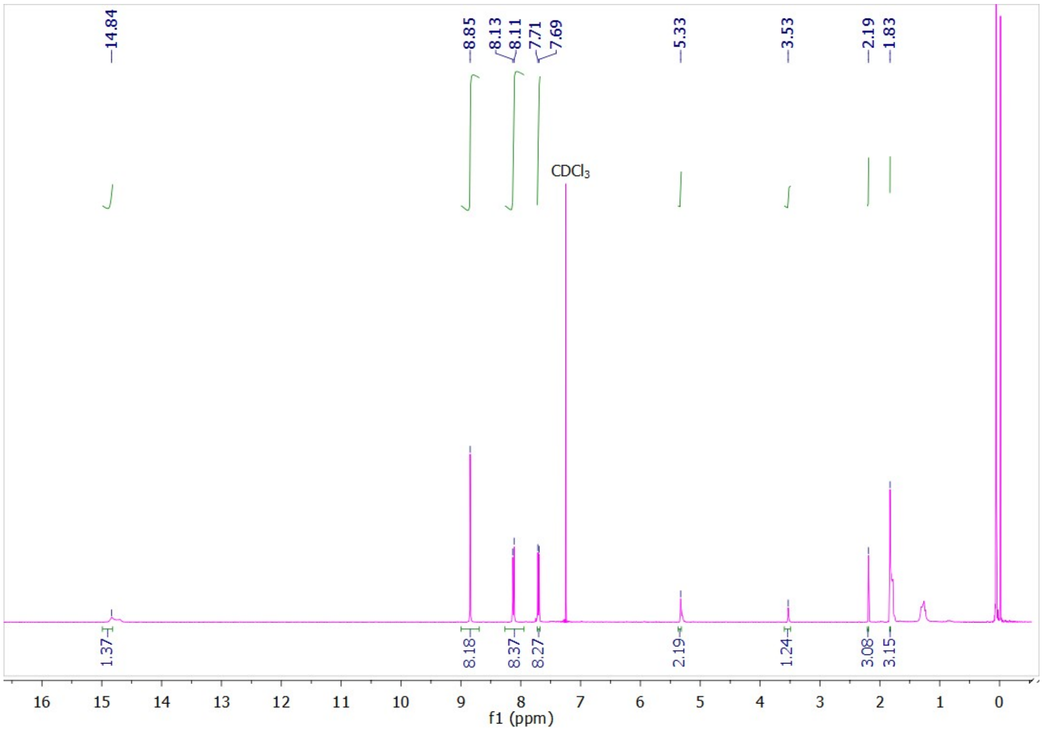

Figure S28. ^{1}H NMR spectrum of catalyst **1** after degradation of MB dye over six cycles.

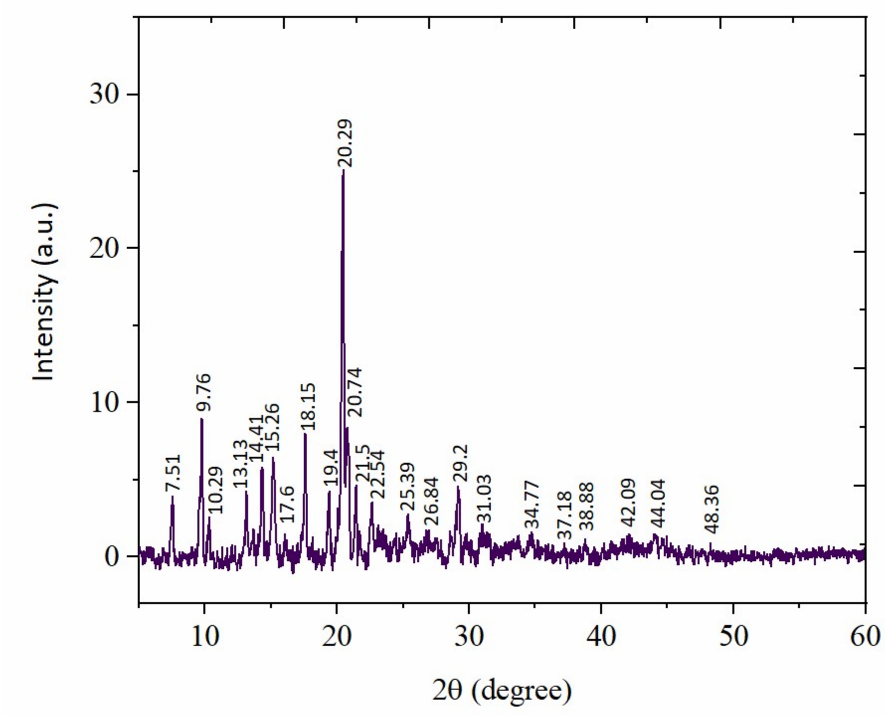

Figure S29. PXRD pattern of catalyst **1** after degradation of CV dye over six cycles.

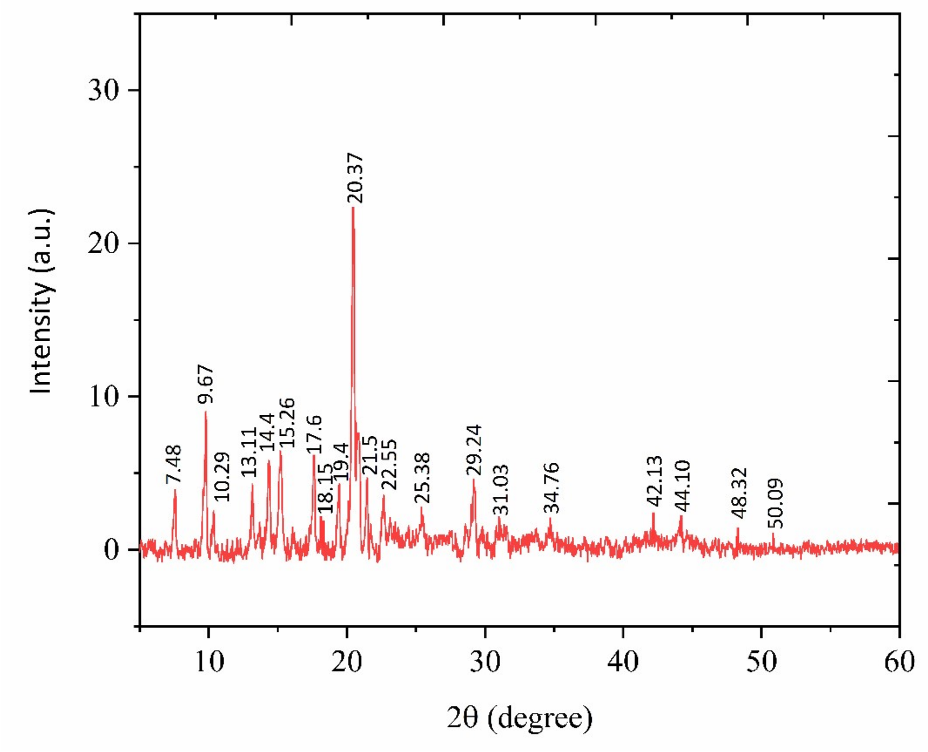

Figure S30. PXRD pattern of catalyst **1** after degradation of MB dye over six cycles.

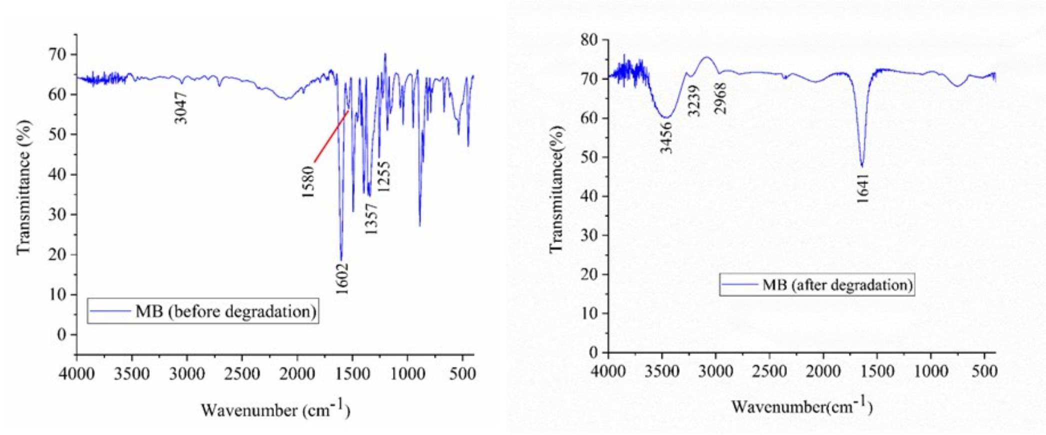

(a) (b)

Figure S31. FTIR spectra of MB dye before degradation (a) and after degradation (b).

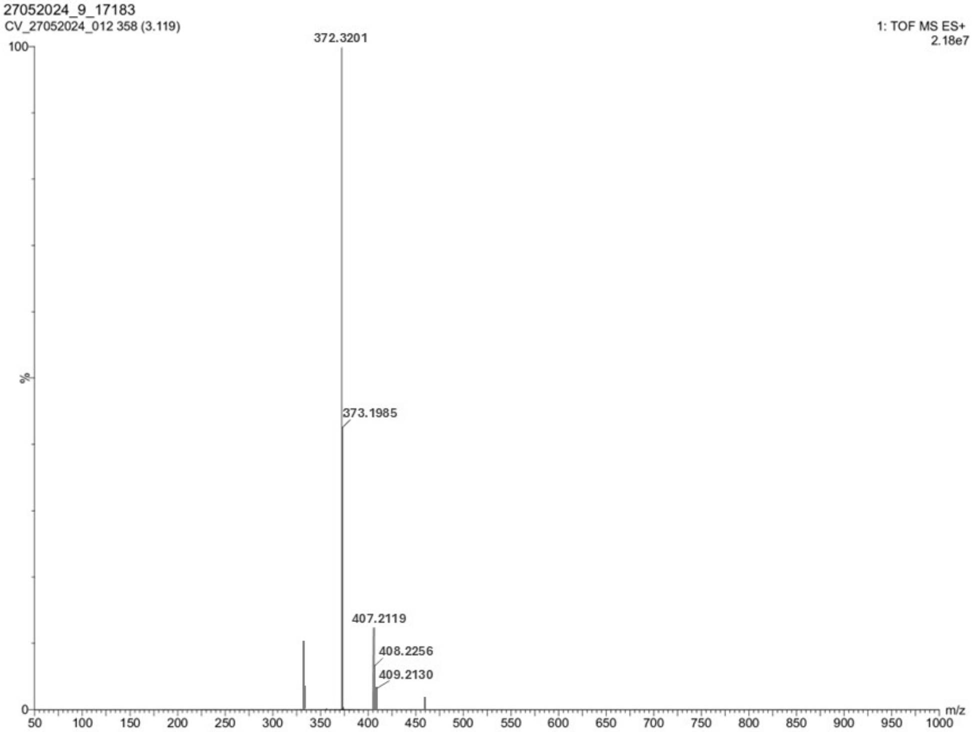

Figure S32. Mass spectra of CV dye before degradation.

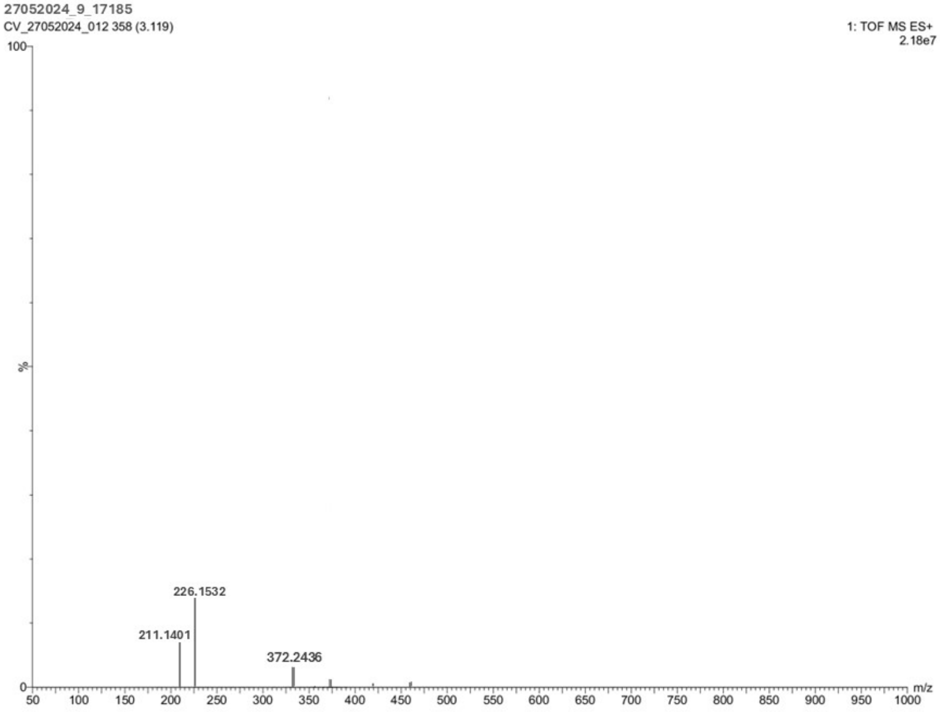

Figure S33. Mass spectra of CV dye's possible fragmentations generated using [MgT(4-Cl)PP(Hacac)] catalyst after degradation.

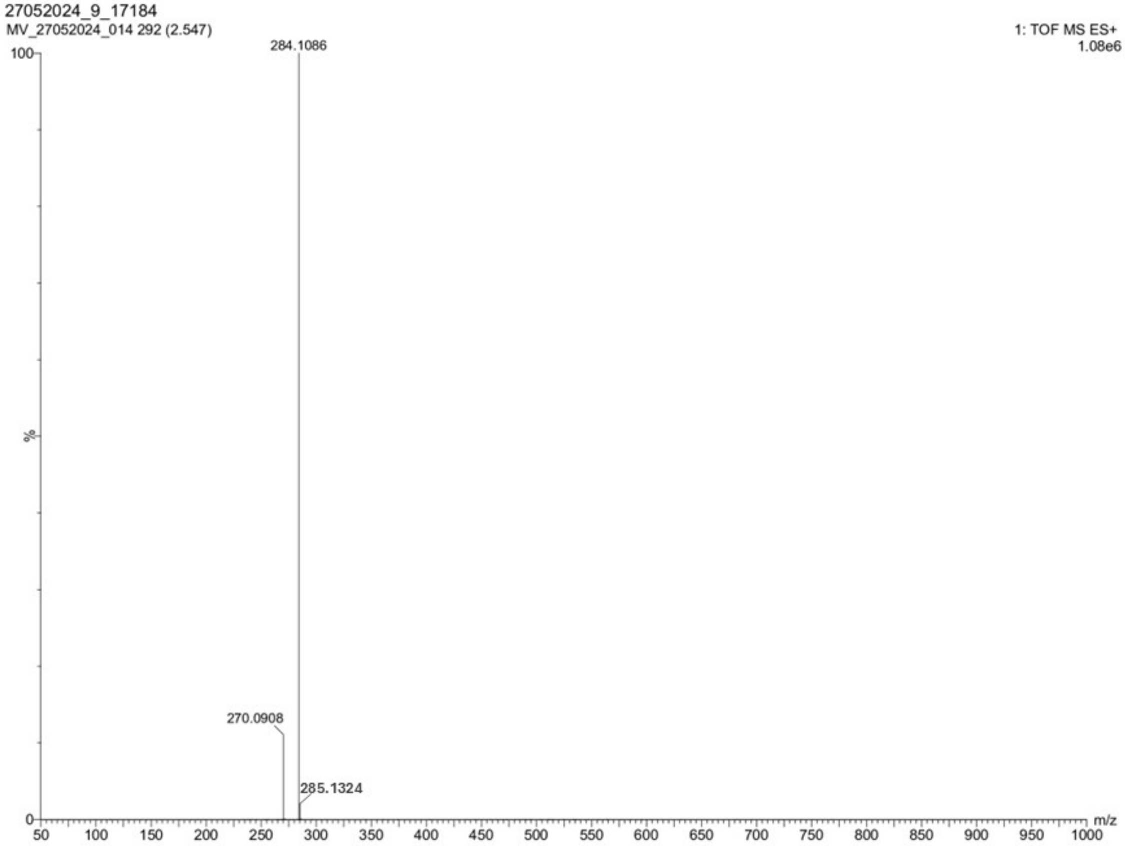

Figure S34. Mass spectra of MB dye before degradation.

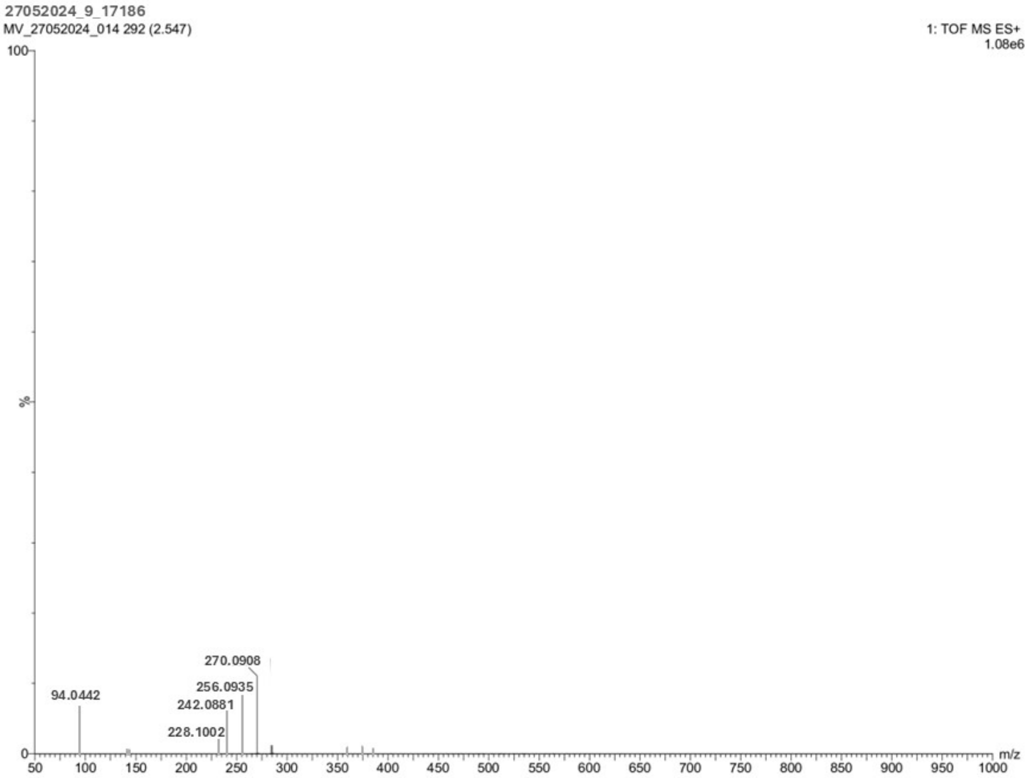

Figure S35. Mass spectra of MB dye's possible fragmentations generated using [MgT(4-Cl)PP(Hacac)] catalyst after degradation.

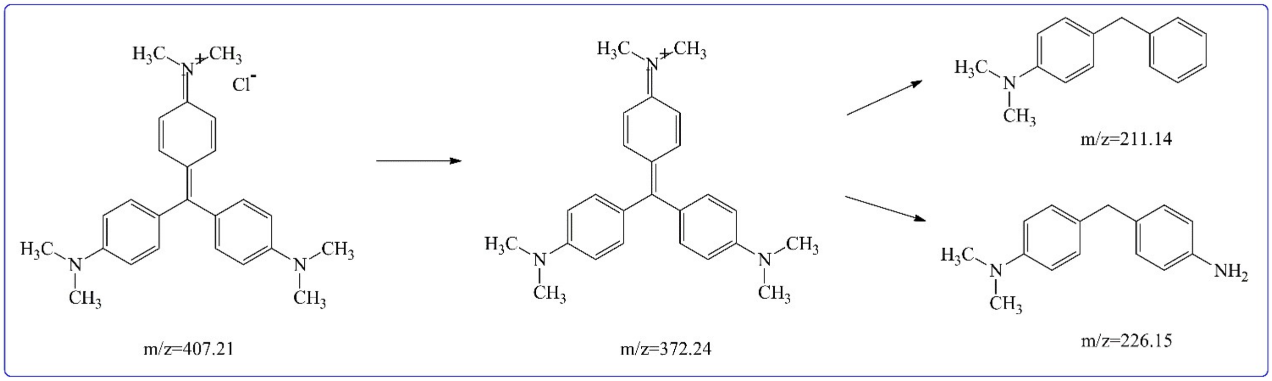

Figure S36. Possible reaction intermediates (obtained with the help of mass spectral data) of CV dye after the photocatalytic reaction using [MgT(4-Cl)PP(Hacac)] and sun light illumination.

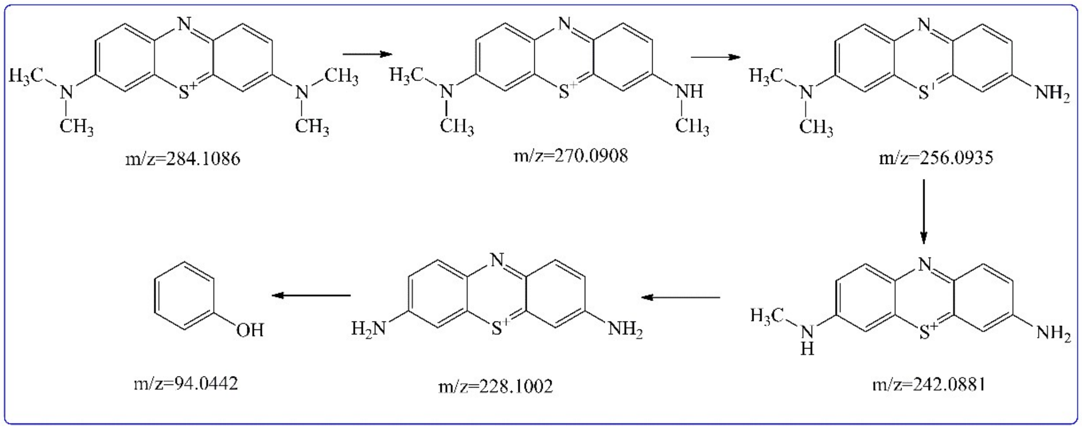

Figure S37. Possible reaction intermediates (obtained with the help of mass spectral data) of MB dye after the photocatalytic reaction using [MgT(4-Cl)PP(Hacac)] and sun light illumination.

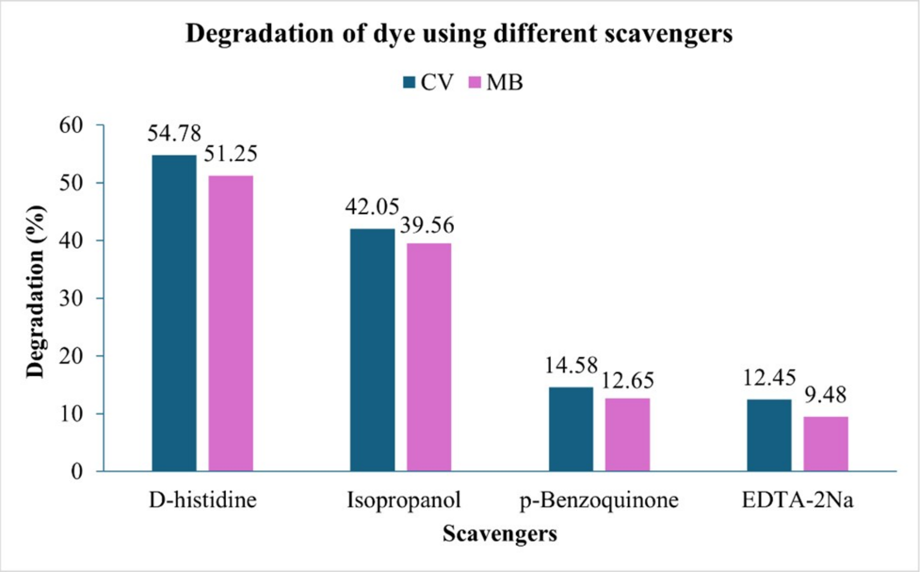

Figure S38. Effect of different scavengers on degradation of CV and MB dyes.

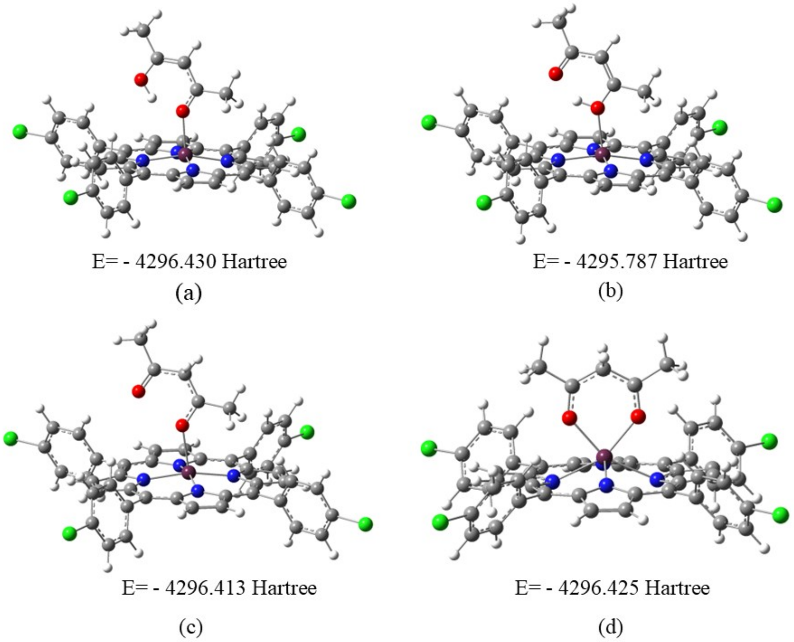

E= - 4296.430 Hartree
(a)

E= - 4295.787 Hartree
(b)

E= - 4296.413 Hartree
(c)

E= - 4296.425 Hartree
(d)

Figure S39. Optimized structures of **1** showing different binding modes with energy.

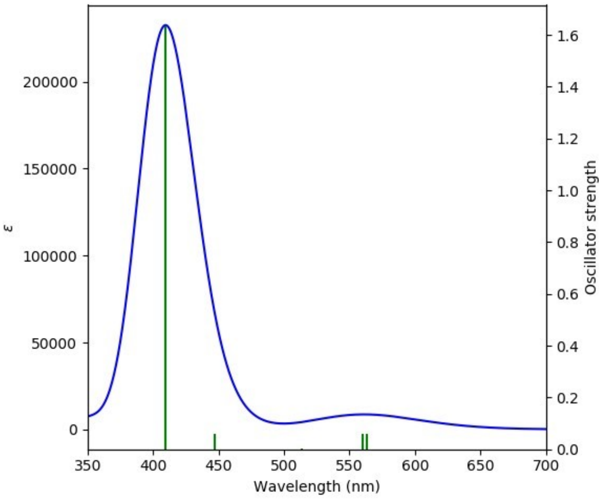

Figure S40. Simulated UV-Vis spectrum of **1.**

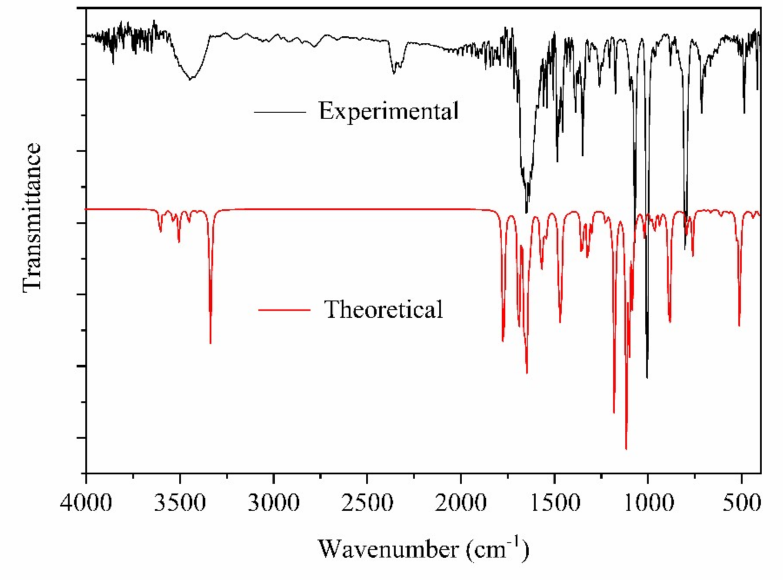

Figure S41. Comparison of experimental and theoretical IR spectra of compound 1.

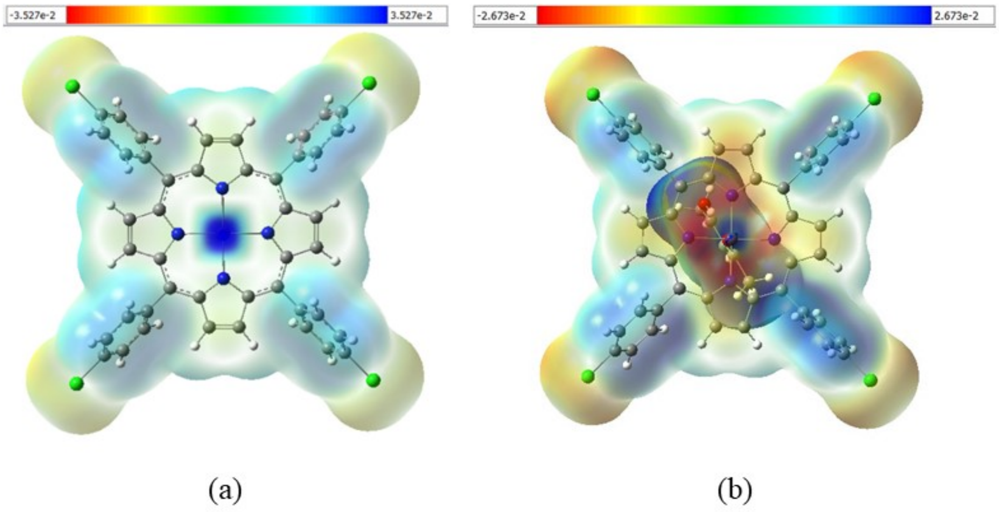

Figure S42. Molecular electrostatic potential (MEP) map of (a) MgT(4-Cl)PP and (b) **1**.